Research Square

Preprints are preliminary reports that have not undergone peer review.
They should not be considered conclusive, used to inform clinical practice,
or referenced by the media as validated information.

Spatial evidence of senescence-associated pathology after myocardial infarction in humans and therapeutic targeting in ageing mice

Rachael E Redgrave
Newcastle University
Eleftherios Zormpas
Newcastle University
Lily Mathison
Newcastle University
Maria Camacho Encina
Newcastle University
Ioakim Spyridopoulos
Newcastle University
Simon J Cockell
Newcastle University
Simon Tual-Chalot
Newcastle University
Gavin David Richardson
gavin.richardson@ncl.ac.uk
Newcastle University

Article

Keywords: cellular senescence, senolytics, navitoclax, myocardial infarction, cardiac ageing, spatial transcriptomics

Posted Date: September 8th, 2026

DOI: https://doi.org/10.21203/rs.3.rs-10930426/v1

License: This work is licensed under a Creative Commons Attribution 4.0 International License.
Read Full License

Additional Declarations: Competing interest reported. Eleftherios Zormpas is currently an employee of Translational Omics, Translational Sciences, GSK, Gunnels Wood Road, Stevenage, SG1 2NY, UK. All other authors declare no financial or non-financial competing interests.

Spatial evidence of senescence-associated pathology after myocardial infarction in humans and therapeutic targeting in ageing mice.

Rachael E Redgrave[1], Eleftherios Zormpas[1,3], Lily Mathison[1], Maria Camacho Encina[1], Ioakim Spyridopoulos[2], Simon J. Cockell[1,3], Simon Tual-Chalot[1], Gavin D Richardson[1]*.

[1]Biosciences Institute, Newcastle University, Newcastle upon Tyne, NE1 3BZ, UK

[2] Translational and Clinical Research Institute, Newcastle University, Newcastle upon Tyne, NE1 3BZ, UK

[3]School of Biomedical, Nutritional and Sport Sciences, Faculty of Medical Sciences, Newcastle University, Newcastle upon Tyne, NE2 4HH, UK

Corresponding author*: Prof. Gavin D. Richardson, Cardiovascular Research Centre, Institute of Genetic Medicine, Newcastle University, Newcastle upon Tyne, NE1 3BZ UK, Telephone: +44 (0)191 241 8615 Fax: +44 (0)191 241 8666 Email Gavin.richardson@ncl.ac.uk

Keywords: cellular senescence; senolytics; navitoclax; myocardial infarction; cardiac ageing; spatial transcriptomics

Abstract

Myocardial infarction predominantly affects older adults, yet whether post-injury senolysis improves repair in a middle-aged heart, and whether senescence-associated pathology is present in human post-infarction myocardium, remain unclear. We treated 15-month-old male mice, an age-relevant middle-aged model, with navitoclax for seven days after ischaemia–reperfusion injury. Navitoclax reduced $p16^{INK4a}$-positive and $p21^{CIP1}$-positive nuclei and was associated with smaller scars, reduced immune-cell accumulation, increased peri-infarct vascularisation and attenuated cardiomyocyte hypertrophy. We also analysed spatial-transcriptomic data from human post-infarction myocardium. Infarct-zone tissue showed increased CDKN2A-positive spot frequency and broader senescence-associated transcriptional activity. Senescence-high niches were enriched for fibrotic and inflammatory programmes, showed altered inferred immune composition and had increased detection of anti-apoptotic BCL-2-family transcripts, including navitoclax targets. To our knowledge, this is the first spatial, multi-gene evidence of a broader senescence-associated programme in pathologically defined human post-infarction myocardium. Together, these findings show that post-injury navitoclax improves histological remodelling in middle-aged mice and support cellular senescence as a candidate therapeutic target after myocardial infarction.

Introduction

Age is a major risk factor for cardiovascular disease and myocardial infarction, yet ST-segment elevation myocardial infarction (STEMI) commonly occurs before advanced old age. UK registry data report a mean age of 65.8 years among patients with STEMI, highlighting the need for preclinical models that extend beyond young adulthood without focusing exclusively on extreme ageing.[1] Myocardial repair becomes progressively impaired with age, increasing susceptibility to adverse remodelling and poor outcomes following infarction.[2,3] Although reperfusion has transformed acute management, age-associated changes in inflammation and reparative capacity continue to constrain recovery.[4] Cellular senescence may contribute to this decline. Senescent cells accumulate in the ageing myocardium[5,6] but can also be induced rapidly by oxidative stress, DNA damage and metabolic dysfunction.[7] Through cell-autonomous dysfunction and the senescence-associated secretory phenotype (SASP), these cells can promote inflammation, fibrosis and impaired tissue repair.[8,9]

Previous senolytic studies have examined complementary aspects of this biology. We demonstrated that two intermittent seven-day courses of navitoclax administered to approximately 24-month-old male mice before permanent left anterior descending coronary artery ligation reduced pre-existing myocardial senescence and age-associated cardiac remodelling.[5] Senolysis markedly improved survival and prevented progressive loss of left ventricular function, but the prophylactic design did not establish whether treatment would remain effective when initiated after myocardial infarction.

We subsequently examined post-injury senolysis following ischaemia–reperfusion in 3- to 4-month-old male mice, selected to minimise the background burden of age-associated senescent cells and isolate the response induced by acute injury.[9] A seven-day course of navitoclax initiated four days after injury reduced senescence-associated markers and inflammatory SASP factors, decreased scar size, increased vascular density and improved cardiac function.[9] This established injury-induced senescence as a therapeutically modifiable component of post-ischaemic damage, but in a young myocardium lacking the pre-existing senescent-cell burden characteristic of ageing.

Complementary evidence was subsequently provided using dasatinib and quercetin in 22- to 24-month-old female mice following permanent LAD ligation.[10] Treatment reduced senescence-associated markers, fibrosis and cardiomyocyte hypertrophy and improved capillary density and ventricular function, although scar size was not significantly reduced. Permanent ligation models produce sustained, unreperfused coronary occlusion and differ from the contemporary clinical setting, in which coronary blood flow is restored, most commonly by primary percutaneous coronary intervention. Permanent ligation and ischaemia–reperfusion produce different infarct architecture, inflammatory responses and patterns of ventricular remodelling.[11,12] Moreover, reperfusion itself produces oxidative and inflammatory injury capable of inducing myocardial senescence.[9] These differences, together with variation in sex, age, senolytic agent and treatment duration, preclude direct comparisons but emphasise the need to evaluate post-injury senolysis in an age-relevant, reperfused heart.

Because navitoclax and dasatinib have clinically important toxicities,[13,14] brief “hit-and-run” senolytic regimens may offer a more translatable strategy than sustained drug exposure.[15] It therefore remained unknown whether a short regimen initiated after reperfusion would improve repair in a middle-aged myocardium containing pre-existing age-associated senescence. Fifteen-month-old mice provide a clinically relevant middle-aged model that is more representative of the typical age of patients presenting with STEMI than young-adult or extremely aged models.[1,16]

A parallel question is whether comparable senescence-associated pathology occurs in human post-infarction myocardium. Earlier studies identified increased senescence-associated markers in cardiac tissue from patients with coronary disease but did not examine pathologically defined infarcted myocardium.[17] More recently, Yang et al. reanalysed the Kuppe et al. human myocardial infarction atlas[18] and reported increased gene-level CDKN2A expression in cardiomyocytes and fibroblasts from infarct-zone tissue.[19] However, gene-level CDKN2A expression cannot distinguish transcripts encoding $p16^{INK4a}$ from $p14^{ARF}$, and expression of a single senescence-associated locus is insufficient to establish cellular senescence.[20,21] That human dataset analysis did not determine whether a broader multi-gene senescence programme was spatially organised within pathological microenvironments associated with fibrosis, inflammation and immune remodelling..

We therefore examined the effects of a seven-day course of navitoclax initiated after cardiac ischaemia–reperfusion injury in 15-month-old male mice. In parallel, we independently analysed the Kuppe et al. human myocardial spatial transcriptomic dataset[18] to determine whether senescence-associated pathology is spatially organised within post-infarction myocardium. Navitoclax reduced myocardial senescence-associated marker burden and adverse structural remodelling while increasing vascular density. Human infarct-zone myocardium showed increased *CDKN2A*-positive spot burden and broader senescence-programme activity, with senescence-rich regions associated with fibrosis, inflammation and altered inferred immune composition. These regions also showed increased detection of anti-apoptotic BCL-2-family genes, including molecular targets of navitoclax. Together, these findings demonstrate that the benefits of short-course post-injury senolysis are retained in middle-aged myocardium and provide, to our knowledge, the first spatial, multi-gene evidence of a broader senescence-associated programme in pathologically defined human post-infarction tissue.

Results

Navitoclax reduces senescence marker burden and attenuates adverse structural remodelling following myocardial ischaemia-reperfusion injury in 15-month-old middle-aged mice.

To determine whether senolytic treatment modifies adverse remodelling after myocardial infarction in middle-aged murine myocardium, 15-month-old male mice were subjected to transient left anterior descending coronary artery ligation for 60 min followed by reperfusion. Navitoclax was initiated four days after ischaemia–reperfusion and continued for seven days, coinciding with the acute post-ischaemic senescence response identified previously.[9] Hearts were collected five weeks after surgery to assess the impact of senolytic treatment on myocardial remodelling (**Fig. 1A**).

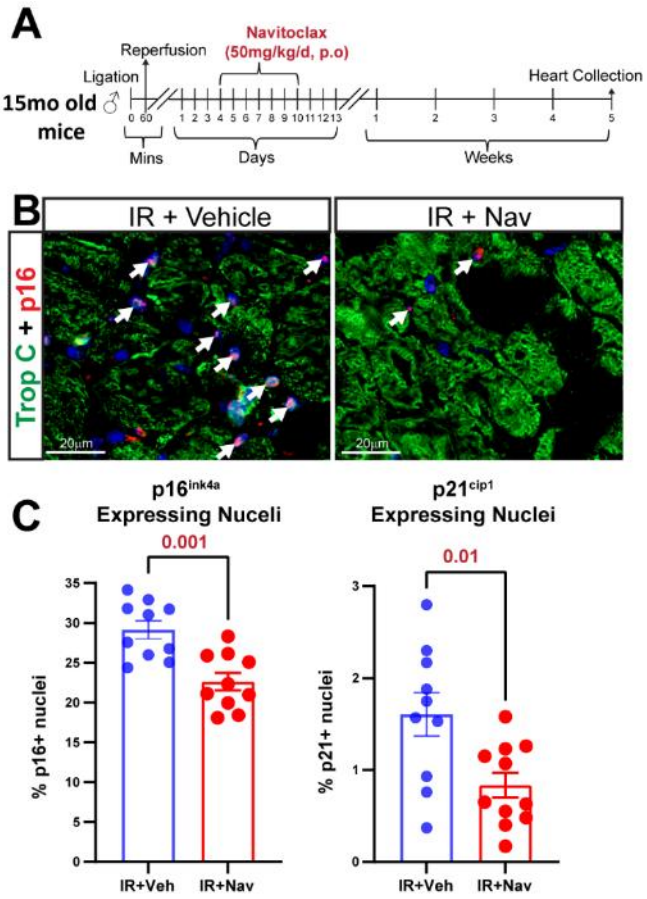


Fig. 1 | Navitoclax reduces myocardial senescence marker burden following ischaemia–reperfusion injury in middle-aged male mice. 15-month-old male mice were subjected to transient coronary artery ligation followed by reperfusion and treated with navitoclax during the early post-injury repair phase. **A.** Experimental timeline showing ischaemia–reperfusion injury, navitoclax treatment and heart collection. **B.** Representative immunofluorescent staining showing p16^{INK4a}-positive nuclei (Red) in vehicle-treated and navitoclax-treated hearts, co-labelled with Troponin C (Trop C; green) and DAPI (blue). **C.** Quantification of p16 ^{inka4}-positive and p21^{CIP1}-positive nuclei following ischaemia–reperfusion injury. Data are shown as individual animals with group means ± SEM. n = 10–11 mice per group. Comparisons between IR + Vehicle and IR + Navitoclax groups were performed using two-tailed unpaired t-tests with Welch's correction. *P*-values are shown above comparisons, with significant values shown in red. IR, ischaemia-reperfusion, Nav, navitoclax, Veh, Vehicle, LV, left ventricle. Scale bars, 20 μm.

We focused on $p16^{INK4a}$ and $p21^{CIP1}$ as senescence-associated markers of myocardial injury and repair. In vehicle-treated middle-aged myocardium, immunofluorescence analysis identified a persistent senescence-associated cell burden during the remodelling phase, with 29.13 ± 1.13% of nuclei positive for $p16^{INK4a}$ and 1.60 ± 0.24% positive for $p21^{CIP1}$ (**Fig. 1B**). Navitoclax reduced both marker-positive populations, lowering $p16^{INK4a}$-positive nuclei to 22.13 ± 1.12% and $p21^{CIP1}$-positive nuclei to 0.83 ± 0.13% (**Fig. 1C**), consistent with reduced myocardial senescence marker burden following senolytic treatment.

Navitoclax was also associated with improved structural repair after ischaemia–reperfusion injury. Masson's trichrome staining showed that scar size was reduced from 18.92 ± 1.08% of left ventricular area in vehicle-treated mice to 13.61 ± 1.88% in navitoclax-treated mice, corresponding to an approximate 28% relative reduction in scar size (**Fig. 2A**). Membrane labelling with wheat germ agglutinin demonstrated reduced cardiomyocyte cross-sectional area following navitoclax treatment, with mean cardiomyocyte area decreasing from 317.4 ± 14.97 μm² to 254.2 ± 14.29 μm², consistent with attenuation of hypertrophic remodelling (**Fig. 2B**). This observation is notable because previous studies in young animals reported no change in cardiomyocyte hypertrophy following ischaemia–reperfusion and senolytic treatment, whereas navitoclax has been shown to attenuate cardiomyocyte hypertrophy in aged, non-ischaemic 24-month-old mice.[6,9]

Navitoclax also significantly increased CD31-positive capillary density following ischaemia–reperfusion injury (**Fig. 2C**). CD31-positive capillary number increased from 55.99 ± 1.66 per field of view in vehicle-treated mice to 64.58 ± 1.75 per field of view in navitoclax-treated mice, corresponding to an absolute increase of 8.59 capillaries per field of view and an approximate 15.3% relative increase ($p = 0.0022$). In young mice, improved post-ischaemic remodelling following navitoclax treatment was proposed to involve suppression of the pro-inflammatory senescence-associated secretory phenotype.[9] Consistent with this mechanism, navitoclax-treated middle-aged mice showed a significant reduction in CD45-positive immune cell burden compared with vehicle-treated controls, decreasing from 8.15 ± 0.40% to 6.81 ± 0.43%, corresponding to an approximate 16.4% relative reduction in immune cells (*p*

= 0.0358; **Fig. 2D**). Together, these histological findings support improved post-ischaemic structural repair following senolytic treatment in the ageing myocardium.

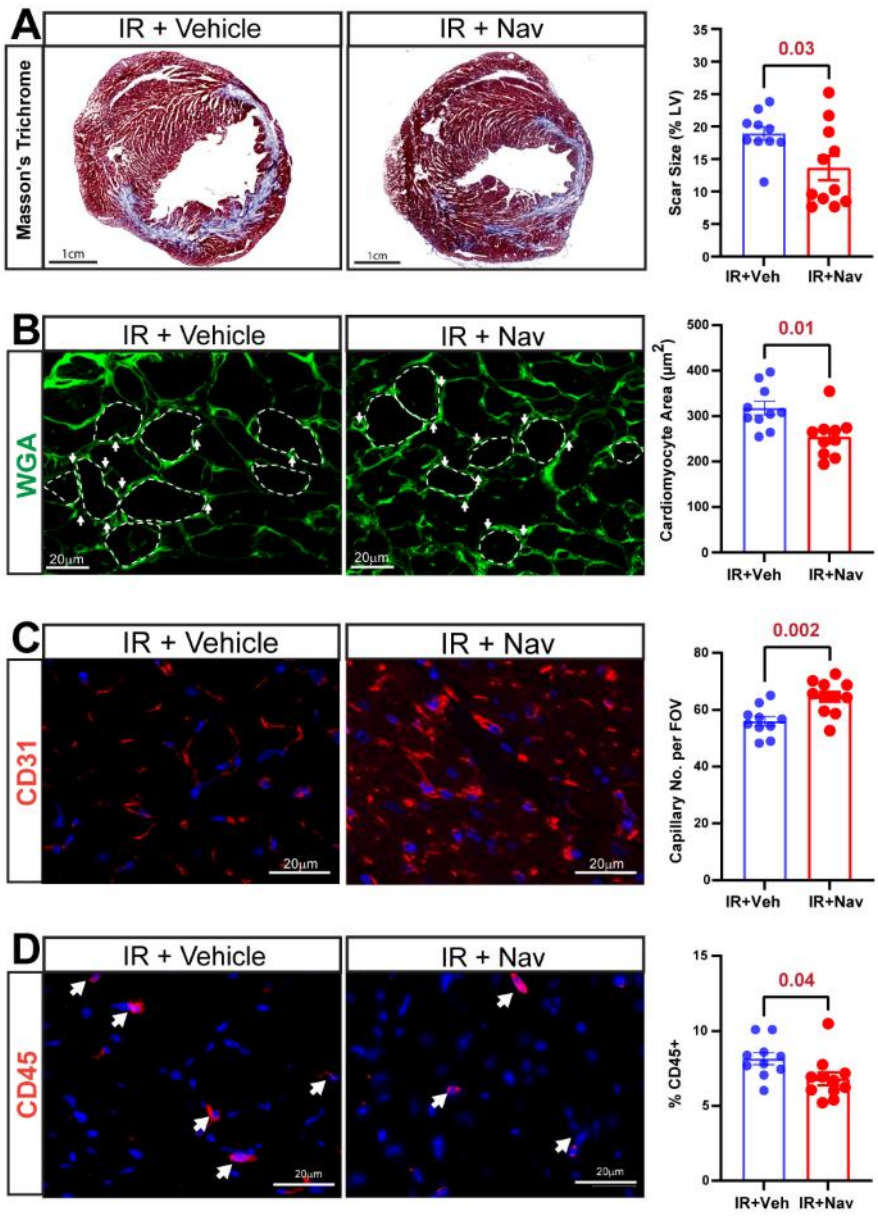


Fig. 2 | Senolytic treatment reduces adverse remodelling following ischaemia–reperfusion in middle-aged male mice. A. Representative Masson's trichrome stained left ventricular sections from vehicle-treated and navitoclax-treated mice, with quantification of infarct scar size expressed as percentage of left ventricular area. **B.** Representative wheat germ agglutinin (WGA) staining of cardiomyocyte membranes, with quantification of cardiomyocyte cross-sectional area. **C.** Representative CD31 immunofluorescence staining (red) with DAPI (blue). Quantification of capillary number per field of view, showing increased capillary density in navitoclax-treated hearts. **D.** Representative CD45 immunofluorescence staining, with quantification of CD45-positive immune cells (red) and DAPI (blue). Data are shown as individual animals with group means ± SEM. n = 10–11 mice per group. Comparisons between IR + Vehicle and IR + Navitoclax groups were performed using two-tailed unpaired t-tests with Welch's correction. P values are shown above comparisons, with significant values shown in red. IR, ischaemia-reperfusion, Nav, navitoclax, Veh, Vehicle, LV, left ventricle, FOV, field of view. Scale bars, as indicated.

Human ischaemic myocardium shows spatial enrichment of senescence-associated programmes.

To assess whether the biology targeted in middle-aged mice is relevant to human disease, we performed a secondary analysis of the published Kuppe et al.[18] human myocardial infarction spatial transcriptomic dataset. Myocardial samples were grouped according to pathology zone, including control myocardium, remote zone and ischaemic/infarct zone Fibrotic-zone samples represented later post-infarction fibrotic remodelling (**Fig. 3A**).

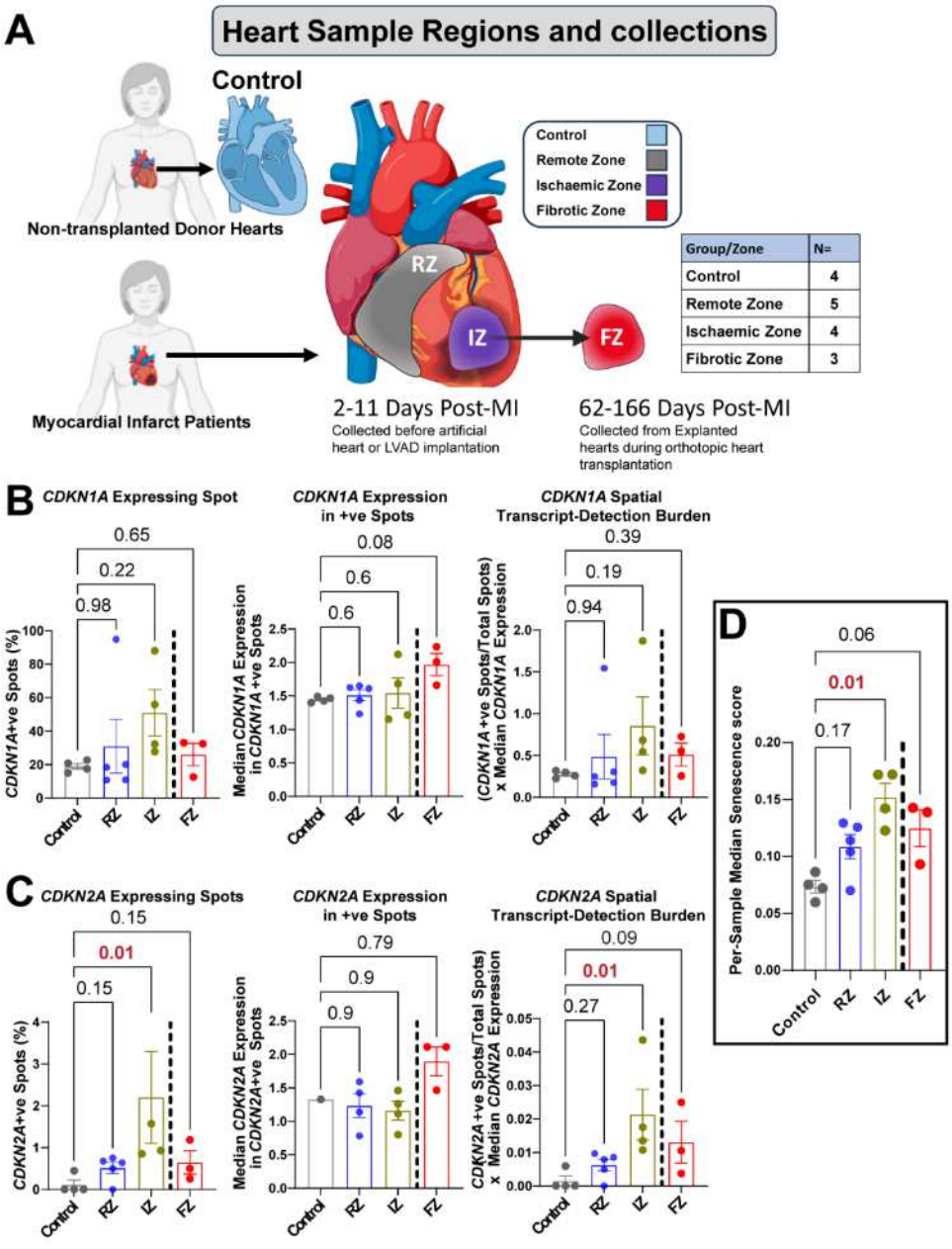


Fig. 3 | Human myocardial infarction spatial transcriptomics identifies enrichment of senescence-associated programmes in pathological myocardial regions. A. Cartoon depicting myocardial samples used for spatial transcriptomics grouped by sample-level pathology-zone origin, including control myocardium, remote zone, RZ, infarct zone, IZ, and fibrotic zone, FZ. The dotted line separating FZ from the other pathology-zone groups indicates that fibrotic zone samples were collected at a later disease stage and therefore represent later-stage post-infarction fibrotic remodelling rather than the same temporal context as the remote and infarct-zone samples. Zone labels refer to the pathological origin of each sample and not to within-section segmentation. **B.** *CDKN1A* analysis across pathology-zone sample groups. Left, detection frequency of *CDKN1A*-positive spots, expressed as the percentage of spatial spots with detectable *CDKN1A* expression. Middle, conditional *CDKN1A* expression intensity, calculated as the median *CDKN1A* expression among *CDKN1A*-positive spots, expression > 0. Right, *CDKN1A* burden, calculated as the fraction of *CDKN1A*-positive spots multiplied by the median *CDKN1A* expression within *CDKN1A*-positive spots. **C.** *CDKN2A* analysis across pathology-zone sample groups. Left, detection frequency of *CDKN2A*-positive spots, expressed as the percentage of spatial spots with detectable *CDKN2A* expression. Middle, conditional *CDKN2A* expression intensity, calculated as the median *CDKN2A* expression among *CDKN2A*-positive spots, expression > 0. Right, *CDKN2A* burden, calculated as the fraction of *CDKN2A*-positive spots multiplied by the median *CDKN2A* expression within *CDKN2A*-positive spots. **D.** Multi-gene senescence programme scores across pathology-zone sample groups. Each point represents one spatial sample and shows the median senescence programme score across all spots in that sample. Graphs show individual spatial samples with group mean ± SEM. Statistical comparisons were performed using Kruskal-Wallis tests followed by Benjamini-Hochberg correction for multiple comparisons. Adjusted *p*-values are shown above comparisons, with significant values shown in red.

We first examined the senescence-associated genes *CDKN1A*, encoding $p21^{CIP1}$, and *CDKN2A*. *CDKN2A* gives rise to multiple transcripts, including those encoding $p16^{INK4a}$ and $p14^{ARF}$; therefore, gene-level CDKN2A expression in the Visium dataset was treated as a senescence-associated signal rather than an isoform-specific measure of $p16^{INK4a}$, across pathology-zone sample groups. Because both genes showed sparse detection at Visium spot resolution, expression intensity was summarised only among marker-positive spots, with the corresponding detection frequency shown separately. This sparse-aware strategy avoided misleading zero-heavy all-spot summaries and allowed us to distinguish between increased marker prevalence and increased expression intensity within marker-positive spots. To integrate these two features, we also calculated spatial marker burden as the fraction of marker-positive spots multiplied by the median expression level within marker-positive spots.

CDKN1A showed variable detection across pathological regions, but *CDKN1A* detection frequency, positive-spot expression intensity and spatial burden were not significantly increased across pathology zones (**Fig. 3B**). In contrast, *CDKN2A* was significantly enriched in ischaemic/infarct-zone samples, with increased *CDKN2A*-positive spot frequency and increased *CDKN2A* burden compared with control myocardium (**Fig. 3C**). Quantitatively, *CDKN2A*-positive spot frequency increased from 0.11 ± 0.11% in control myocardium to 2.2 ± 1.10% in infarct-zone myocardium, corresponding to an approximate 19.7-fold increase. *CDKN2A* spatial burden showed a similar pattern, increasing from 0.0015 ± 0.0015 in control myocardium to 0.0214 ± 0.0075 in infarct-zone myocardium. These effect-size estimates support the interpretation that infarct-zone myocardium contains an expanded *CDKN2A*-positive spatial compartment rather than simply higher transcript abundance within a small number of positive spots. *CDKN2A* expression intensity within positive spots was not significantly altered, indicating that the increased burden was driven primarily by a greater proportion of *CDKN2A*-positive spatial spots rather than higher expression within individual positive spots. This pattern is biologically consistent with senescence-associated *CDKN2A* activation. In healthy myocardium, most cardiac and stromal cells would be expected to have low or undetectable *CDKN2A* expression,[6,19] whereas senescence induction would be expected to increase the number of *CDKN2A*-positive cells or local cellular niches. Therefore, the increased prevalence of *CDKN2A*-positive spots, rather than higher expression intensity within already positive spots, supports the interpretation that ischaemic injury is associated with expansion of senescence-associated spatial contexts in human infarct-zone myocardium. However, because each Visium spot can contain multiple cells, this finding should be interpreted as increased spatial detection of *CDKN2A*-associated senescence signal rather than definitive single-cell identification of senescent cells.

We next assessed a broader multi-gene senescence programme score across all spots using a cardiac-expressed SenMayo-derived[22] panel expanded with selected senescence-associated genes (**supplementary data 1**). This provided a complementary readout that was less dependent on sparse detection of individual senescence-associated genes and, importantly, did not rely on interpreting gene-level CDKN2A expression as an isoform-specific measure of $p16^{INK4a}$. SenMayo scoring confirmed significant enrichment in the ischaemic/infarct zone compared with control

myocardium (**Fig. 3D**). Because module scores are relative transcriptional programme scores rather than direct percentages, we summarised the effect as an absolute difference rather than a percentage change. The senescence programme score increased from 0.0735 ± 0.0055 in control myocardium to 0.1523 ± 0.0121 in infarct-zone myocardium, corresponding to an absolute increase of 0.0788 score units. Fibrotic zone samples also showed a numerically higher senescence programme score than controls, increasing from 0.0735 ± 0.0055 to 0.1250 ± 0.0160, although this comparison did not reach statistical significance (**Fig. 3D**; $p = 0.06$), possibly because the fibrotic zone represents a later-stage remodelling region in which the infarcted myocardium has undergone extensive cell loss, extracellular matrix deposition and scar maturation. Consistent with this interpretation, previous murine ischaemia-reperfusion data showed that senescence is induced early after injury, is prominent during the acute post-ischaemic period, and is reduced but remains detectable at later remodelling time points.[9] Together, these findings suggest that senescence programmes are most clearly enriched within acutely injured human post-infarction myocardium, particularly the ischaemic/infarct zone.

We next asked whether senescence-high spatial contexts were associated with altered inferred proportions of resident myocardial cell populations. Senescence-high spots were defined within ischaemic/infarct and fibrotic zones using the composite senescence programme score, and cell2location-derived cell-type proportions[23] were compared between senescence-high and corresponding non-high spots at sample level (**Supplementary Fig. 1**). This exploratory analysis was restricted to resident myocardial structural cell types, as immune-cell composition was examined separately using the spatial neighbourhood analysis described below. No comparison reached statistical significance; however, senescence-high fibrotic regions showed trends towards lower inferred cardiomyocyte proportions and higher fibroblast and smooth-muscle-cell proportions. These observations should be interpreted cautiously given the small sample size, the spatial resolution of Visium data and the secondary nature of the analysis. Importantly, these data represent inferred cell-type proportions within spatial spots and do not identify the senescent cell type directly.

Human senescence-rich spatial regions are associated with fibrosis, inflammation and altered inferred immune composition

The observed trends towards altered resident myocardial cell composition, together with the murine data showing reduced scar size and reduced CD45-positive immune-cell burden following navitoclax treatment, led us to investigate more directly the spatial relationship between senescence-associated programmes, fibrosis, inflammation and immune composition in human myocardial samples. For these neighbourhood analyses, senescence-rich seed spots were defined as the top quartile of multi-gene senescence programme score within each sample and pathology zone. Neighbouring spots were defined as non-seed spots located within twice the median nearest-neighbour spot distance, while all remaining non-seed spots were classified as other spots (**Fig. 4A**). These spatial classes were mutually exclusive.

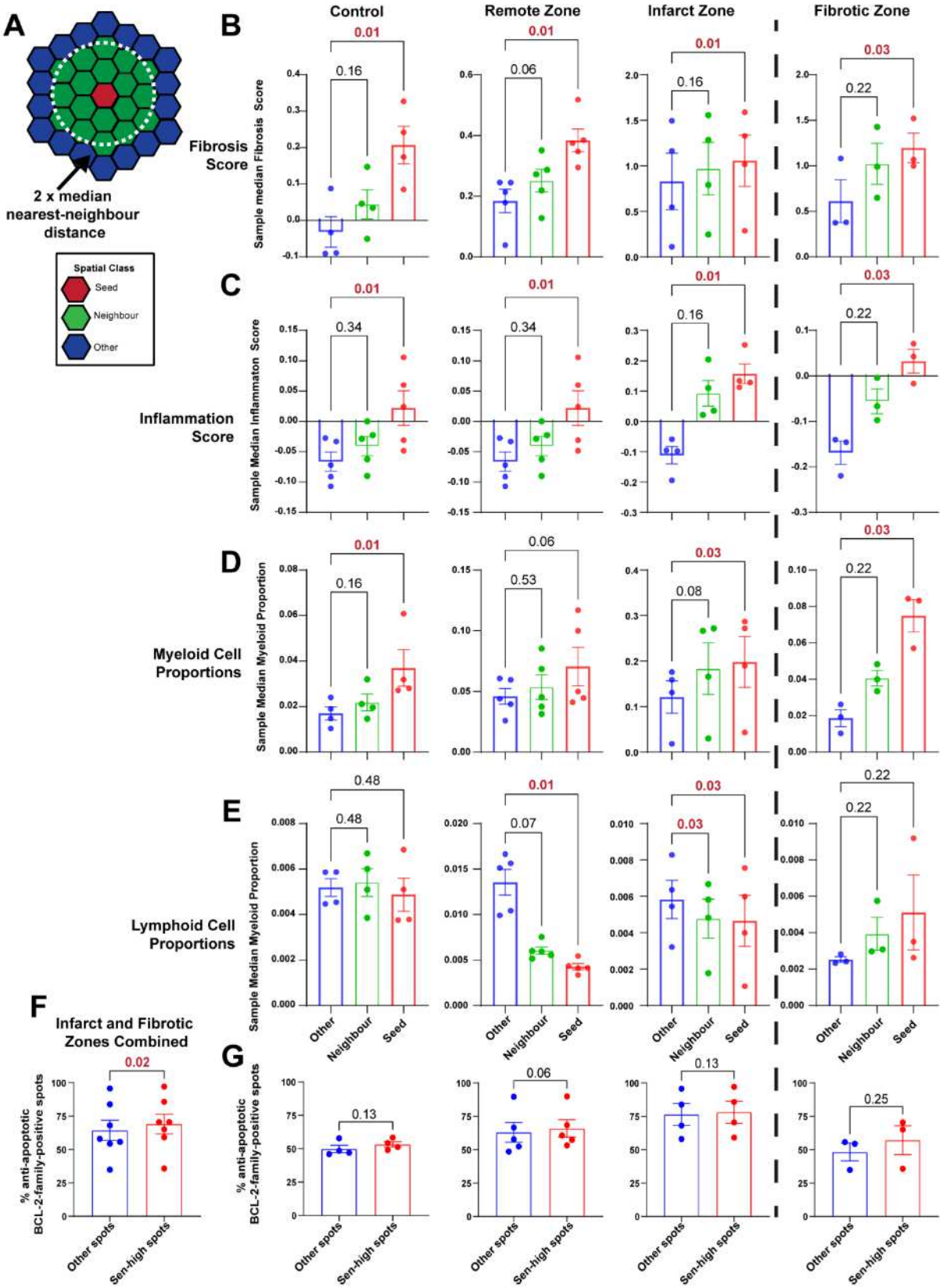

A
2 x median nearest-neighbour distance
Spatial Class
Seed
Neighbour
Other
B
Control
Remote Zone
Infarct Zone
Fibrotic Zone
Fibrosis Score
Sample median Fibrosis Score
C
Inflammation Score
Sample Median Inflammation Score
D
Myeloid Cell Proportions
Sample Median Myeloid Proportion
E
Lymphoid Cell Proportions
Sample Median Myeloid Proportion
Other
Neighbour
Seed
F
Infarct and Fibrotic Zones Combined
% anti-apoptotic BCL-2-family-positive spots
Other spots
Sen-high spots
G
% anti-apoptotic BCL-2-family-positive spots
Other spots
Sen-high spots

Fig. 4 | Human senescence-rich spatial regions are associated with fibrosis, inflammation, altered inferred immune composition and anti-apoptotic *BCL-2*-family gene detection. A) Spatial neighbourhood analysis of senescence-rich regions across human myocardial pathology zones. Senescence-rich seed spots were defined as the top quartile of multi-gene senescence programme score within each sample and pathology zone. Neighbouring spots were defined as non-seed spots located within 2 times the median nearest-neighbour spot distance from at least one seed spot. Other spots were defined as all remaining non-seed spots. These spatial classes were mutually exclusive. **B, C, D and E**) Fibrosis programme score, inflammation programme score, and Kuppe et al. cell2location-derived inferred myeloid and lymphoid cell proportions were quantified across control myocardium, remote zone, fibrotic zone and infarct zone samples. Each point represents one spatial sample and shows the median feature value within the indicated spatial class. Bars show group mean ± SEM across spatial samples. Statistical comparisons between Other, Neighbour and Seed spatial contexts were performed using Friedman tests with Benjamini-Hochberg correction for multiple comparisons. Adjusted *p*-values are shown above comparisons, with significant values highlighted in red. **F)** Spots from infarct-zone and fibrotic-zone samples were stratified within each sample and pathology zone into senescence-high spots, defined as the top quartile of senescence score, and remaining other spots. The percentage of spots positive for at least one anti-apoptotic *BCL-2*-family gene was calculated using *BCL2, BCL2L1, BCL2L2, MCL1* and *BCL2A1.* Each point represents one sample-zone pair. Bars show mean ± SEM. Statistical comparison was performed using a paired Wilcoxon matched-pairs signed-rank test. **G)** Zone-level analysis of anti-apoptotic *BCL-2*-family-positive spot frequency in control myocardium, remote zone, infarct zone and fibrotic zone samples. Each point represents one spatial sample. Bars show mean ± SEM. Statistical comparisons were performed using paired Wilcoxon matched-pairs signed-rank tests comparing other and senescence-high spots within matched sample-zone pairs. With significant values shown in red.

Using this approach, senescence-rich seed spots showed significant enrichment of the fibrosis programme score across pathology zones, including control myocardium (**Fig. 4B**). In control myocardium, fibrosis scores were also increased in spots neighbouring senescence-rich seeds compared with other spatial contexts. We next assessed inflammatory and immune-associated spatial features. Inflammation programme activity was enriched in or near senescence-rich spots across pathology zones, again including control myocardium (**Fig. 4C**). Inferred myeloid proportions were significantly increased within senescence-rich spots across all zones except the remote zone, where a similar trend was observed, $p = 0.054$ (**Fig. 4D**). By contrast, inferred lymphoid proportions were significantly reduced within senescence-rich spots and neighbouring spots in both the remote and infarct zones (**Fig. 4E**). This pattern

suggests that senescence-rich spatial contexts are associated with a relative shift towards innate immune and tissue-remodelling features, although inferred lymphoid depletion should be interpreted cautiously because cell-type proportion estimates are compositional and may partly reflect increased local myeloid abundance.

Senescence-high myocardial spots are enriched for anti-apoptotic BCL-2-family gene detection

Given the beneficial effects of navitoclax treatment observed in aged mice following ischaemia–reperfusion, and in prior studies targeting myocardial senescence,[5,6,9] we next asked whether senescence-enriched regions in human myocardium showed evidence of anti-apoptotic *BCL-2*-family gene detection. Senescent cells are characterised by increased resistance to apoptosis, and senolytic strategies exploit this dependency by targeting pro-survival pathways.[24,25] We therefore focused on the relationship between spatial senescence burden and anti-apoptotic *BCL-2*-family gene detection, rather than asking whether these genes were simply enriched in a particular disease zone.

To test this, spots were stratified within each sample and pathology zone into senescence-high spots, defined as the top quartile of senescence score, and the remaining other spots. We then calculated the proportion of spots positive for at least one anti-apoptotic *BCL-2*-family gene, including *BCL2*, *BCL2L1*, *BCL2L2*, *MCL1* and *BCL2A1*. Because our primary question was whether anti-apoptotic survival signalling was associated with senescence-high spatial niches in human post-infarction pathology, we first focused on injured and remodelled myocardial regions by pooling within-sample comparisons from infarct- and fibrotic-zone sections. This approach avoids over-interpreting small zone-specific sample numbers while testing whether anti-apoptotic *BCL-2*-family gene detection is enriched in senescence-high regions within pathological post-infarction tissue.

Across pooled infarct and fibrotic zones, senescence-high spots contained a significantly greater proportion of anti-apoptotic *BCL-2*-family-positive spots than other spots. Anti-apoptotic *BCL-2*-family-positive spot frequency increased from 64.4 ± 7.66% in other spots to 69.1 ± 7.38% in senescence-high spots ($p = 0.0156$**; Fig. 4F**). We next examined each pathology-zone group separately. Although individual zone-

level comparisons did not reach statistical significance, the direction of effect was consistent across control, remote, infarct and fibrotic zone samples, with senescence-high spots showing numerically higher anti-apoptotic *BCL-2*-family gene detection in each zone (**Fig. 4G**). Together, these data indicate that senescence-enriched human myocardial niches are associated with increased detection of anti-apoptotic BCL-2-family genes, supporting the concept that senescence-high regions engage pro-survival pathways relevant to senolytic vulnerability.

Discussion

This study shows that the beneficial effects of short-course post-injury navitoclax are retained in middle-aged myocardium following myocardial infarction with reperfusion. Reduced myocardial $p16^{INK4a}$ and $p21^{CIP1}$ marker burden was accompanied by smaller scars, attenuated cardiomyocyte hypertrophy, reduced immune-cell accumulation and increased vascular density. These coordinated changes suggest that senescence influences several interconnected components of post-infarction repair rather than scar formation alone. Complementary human spatial analysis identified senescence-associated pathological niches within post-infarction myocardium, providing human disease context for the processes modified by navitoclax in mice.

The current study extends previous investigations of senolysis after myocardial infarction[5,9,10] by showing that the brief post-injury navitoclax regimen previously effective in young mice remains beneficial following reperfused injury in a middle-aged male heart containing pre-existing age-associated senescence. The reduction in cardiomyocyte hypertrophy may be particularly relevant to this aged context because this response was absent from our previous young ischaemia–reperfusion study but has been observed following senescent-cell clearance in aged myocardium.[6,9] This could reflect effects on pre-existing age-associated senescent cells as well as cells entering senescence following injury.

The human analysis extends the limited evidence for senescence within pathologically defined post-infarction myocardium.[19] Importantly, these samples were obtained from patients with clinically managed acute myocardial infarction in the contemporary reperfusion and revascularisation era,[4,18] increasing the translational relevance of comparison with our murine ischaemia–reperfusion model. *CDKN2A*-positive spot

frequency and spatial burden were increased in infarct-zone tissue, whereas expression intensity within positive spots was unchanged.

This suggests expansion of *CDKN2A*-associated spatial contexts rather than simply greater expression within regions already expressing *CDKN2A*. This human finding aligns with previous genetic studies in young mice, in which cardiomyocyte-specific inactivation of cdkn2a/p16^{INK4a} improved cardiac function and reduced scar size following ischaemia–reperfusion, while attenuating senescence-associated inflammation and senescence markers in other myocardial lineages.[8] *CDKN1A* was not significantly increased, highlighting the heterogeneity of senescence-associated states as previously described.[26] Our finding of increased *CDKN2A*-positive spot frequency and spatial burden in infarct-zone myocardium is consistent with the analysis of Yang et al., who also reported increased *CDKN2A* expression following myocardial infarction in the Kuppe et al. dataset.[19] However, gene-level *CDKN2A* expression cannot distinguish between transcripts encoding p16^{INK4a} and p14^{ARF}. We therefore interpreted *CDKN2A* as a senescence-associated signal rather than an isoform-specific marker of p16^{INK4a}, and complemented this analysis with a broader multi-gene senescence programme. This programme was independently enriched in infarct-zone myocardium, providing evidence for a broader senescence-associated transcriptional response rather than reliance on *CDKN2A* expression alone. Senescence-rich regions were also associated with fibrosis, inflammation, increased inferred myeloid proportions and relative lymphoid depletion.

The latter finding should be interpreted as a compositional shift towards innate immune and tissue-remodelling features rather than direct evidence of lymphocyte exclusion. To our knowledge, this study therefore provides the first spatial characterisation of broader senescence-associated niches within pathologically defined human post-infarction myocardium and demonstrates their association with fibrotic, inflammatory and immune-remodelling features. Notably, associations between senescence-rich spatial contexts and increased fibrosis and inflammation programme scores were also evident in control myocardium. In the absence of acute infarction, these regions may reflect senescence accumulating during normal ageing or across the lifespan. Their association with fibrotic and inflammatory transcriptional programmes suggests that these features are not restricted to injury-induced or disease-associated senescence.

Instead, age-associated myocardial senescence may similarly establish local pro-inflammatory and profibrotic tissue environments, supporting the concept that senescent cells can contribute to progressive myocardial remodelling and dysfunction even in the absence of an acute ischaemic insult.

Anti-apoptotic *BCL-2* family transcript detection was also modestly but significantly increased in senescence-high regions when infarct and fibrotic zones were pooled. This is translationally relevant because navitoclax targets *BCL-2*, *BCL-XL* and *BCL-W*, exploiting the dependence of senescent cells on anti-apoptotic pathways.[25] However, transcript detection cannot establish protein abundance, functional dependence or sensitivity to navitoclax. These data therefore support the biological plausibility of targeting related pro-survival pathways in human post-infarction myocardium but do not demonstrate that the identified human niches would respond to navitoclax.

Several limitations should be acknowledged. The mouse study included only male mice at one age and endpoint, and reduced $p16^{INK4a}$ and $p21^{CIP1}$ positivity indicates reduced senescence-associated marker burden rather than definitive selective elimination of senescent cells. The human analysis was conducted at spot rather than single-cell resolution, and inferred cell-type proportions represent relative spatial enrichment. Mouse hearts were examined five weeks after injury, whereas the human samples represented different acute and later post-infarction stages; the two datasets therefore show process-level alignment rather than direct temporal or mechanistic equivalence.

Safety and treatment duration will be central to the clinical translation of senolytic therapy. Navitoclax produces on-target thrombocytopenia through BCL-XL inhibition[13], while dasatinib has been associated with clinically important cardiopulmonary toxicities, including pulmonary arterial hypertension, during longer-term oncology use.[14] These toxicities cannot be directly extrapolated to short senolytic regimens, but they reinforce the attraction of a “hit-and-run” approach in which transient drug exposure is used to remove senescent cells rather than requiring sustained pathway inhibition.[15] Importantly, the improvements observed here were present several weeks after the seven-day treatment course had ended, supporting the possibility that a brief intervention can modify subsequent myocardial remodelling

while limiting cumulative drug exposure. Nevertheless, platelet effects, cardiovascular safety, optimal timing and durability of benefit will require direct evaluation, alongside the development of safer and more selective senolytic agents.

Despite these limitations, the study narrows an important translational gap by showing that a brief post-injury senolytic regimen improves histological remodelling in a middle-aged heart following reperfusion. By connecting this intervention with spatial, multi-gene evidence of a broader senescence-associated programme in human post-infarction myocardium, the findings support further development of safer and more selective senolytic strategies for myocardial repair.

Methods

Animals and ethical approval

All animal procedures were approved by Newcastle University Animal Welfare and Ethical Review Body and performed under UK Home Office Project Licence PP2119777 in accordance with the Animals (Scientific Procedures) Act 1986 and associated guidelines. The study is reported in accordance with the ARRIVE guidelines.

Animals, Procedures and Senolytic Treatment.

Pre-operative medication consisted of fentanyl (0.05 mg/kg) and midazolam (0.5 mg/kg) to provide intra-operative analgesia and sedation. Mice were anaesthetised using isoflurane, intubated, and maintained on mechanical ventilation delivered via a RoVent Advance small-animal ventilator (Kent Scientific).

A left-sided thoracotomy was performed at the fourth intercostal space, permitting partial removal of the pericardium and placement of a 7-0 prolene suture around the left anterior descending artery (LAD). Myocardial infarction was induced by inserting 2 mm PE-10 tubing into the suture loop and tightening the knot to occlude coronary blood flow for 60 minutes. After the occlusion period, the tubing was removed to allow reperfusion, and the thoracic cavity was closed. Buprenorphine (0.1 mg/kg) was administered post-operatively to provide sustained analgesia.

In vivo navitoclax (ABT263) treatment.

Navitoclax was prepared in a lipid vehicle solution consisting of ethanol, polyethylene glycol 400 and Phosal 50 PG in a 1:3:6 ratio, respectively.[27] Mice were randomly assigned to experimental groups. Navitoclax was administered by oral gavage at 50 mg/kg/day[9,27] during the post-injury repair phase, as detailed in the main experimental timeline (**Fig. 1A**) and control animals received vehicle alone. Hearts were collected five weeks after injury for histological assessment of senescence marker burden, scar formation, cardiomyocyte hypertrophy, vascular density and immune cell infiltration.

Immunofluorescence and Histological Analysis

Hearts were equilibrated in 30% sucrose at 4°C and cryoembedded in optimal cutting temperature (OCT) compound (Cellpath). Transverse 10 µm cryosections were mounted on Superfrost Plus Adhesion slides (Epredia). For immunofluorescence, sections were post-fixed in 4% paraformaldehyde (PFA; Thermo Fisher Scientific) for 20 min, permeabilised in 0.5% Triton X-100 (Sigma-Aldrich), and blocked in 10% donkey serum / 1% bovine serum albumin (BSA; Sigma-Aldrich). Primary antibodies were applied overnight at 4°C: rabbit anti-$p16^{INK4a}$ (1:400; ab211542, Abcam), rat anti-$p21^{CIP1}$ (1:200; ab107099, Abcam), rat anti-CD31 (550274, BD Pharmingen), and rat anti-CD45 (1:100; 103102, BioLegend). After washing, sections were incubated with species-appropriate secondary antibodies: anti-rabbit Alexa Fluor 488 (A21206, Invitrogen), donkey anti-rat Alexa Fluor 594 (A21209, Invitrogen), and donkey anti-rat Alexa Fluor 568 (A78946, Invitrogen). Slides were mounted in ProLong Gold Antifade Mountant with DAPI (P36931, Invitrogen). Marker expression was quantified within the peri-infarct region of the left ventricular free wall. Cardiomyocyte hypertrophy was assessed using fluorescein-conjugated wheat germ agglutinin (WGA) (FL-1021-5, Vector Laboratories) to label cell membranes. Only cardiomyocytes within the peri-infarct region that were surrounded by capillaries displaying a cross-sectional profile were analysed, ensuring that WGA labelled cells were in true transverse orientation.

Images were acquired using an AxioImager M2 microscope (Zeiss) and processed in ZEN 2.3 (Zeiss). Quantification was performed using ZEN 2.3 or ImageJ (NIH) depending on the staining protocol. A minimum of 24 images per heart, taken across 3 sections, were analysed (approximately 2000 cells per heart). For each image,

DAPI-labelled nuclei were counted to determine total cell number, and marker-positive cells were quantified as a percentage of this total.

To assess mature scar size at 5 weeks post-reperfusion, every 10th section from ligature to apex was stained using a Masson's Trichrome Stain Kit (HT15-KT, Sigma Aldrich) according to the manufacturer's instructions and imaged using an Aperio CS5 slide scanner (Leica Biosystems). Whole section images were analysed in ImageJ, and scar size was expressed as percentage of total left ventricle. All analyses were performed blinded to treatment group.

Human myocardial spatial transcriptomic analysis.

This secondary analysis used de-identified, publicly available human data; ethical approval and informed consent for tissue collection were obtained in the original study as described by Kuppe et al. [18] No new participants were recruited for the present study. Human myocardial spatial transcriptomic data were analysed in R using per-sample Seurat objects provided with the raw data by the original authors. Sample metadata were used to assign each sample to its pathology-zone origin: control myocardium, remote zone (RZ), infarct zone (IZ) or fibrotic zone (FZ). These pathology-zone labels were analysed as sample-level tissue origins and not as within-slide regional segmentations.

A light-touch spot-level quality-control workflow was applied before downstream analysis. For each sample, spots were summarised by total counts, detected features and the percentage of mitochondrial, haemoglobin and ribosomal transcripts. Spots were retained if they had ≥200 total counts, ≥200 detected features and ≤35% mitochondrial transcripts. Extreme upper-tail count and feature outliers above the 99.5th percentile within each sample were excluded.

Senescence panel: The 95-gene panel comprised 80 genes from the original SenMayo signature[22]. To prioritize genes with evidence of cardiac expression, we used median gene expression values from the Genotype-Tissue Expression (GTEx) project, a large-scale resource that provides RNA sequencing data across multiple human tissues.[28] The original SenMayo signature was filtered based on median transcript abundance in left ventricular tissue, retaining genes with a median

expression value above 0.1 transcripts per million (TPM). The expression threshold was applied to exclude genes with little or no detectable expression in the left ventricle. From these, a subset of 80 genes was selected for downstream analysis.

Because SenMayo intentionally excluded the canonical senescence-associated cell-cycle inhibitors CDKN1A and CDKN2A, these genes were reintroduced, together with four additional genes present in FRIDMAN_SENESCENCE_UP (IFNG, IRF7, SOD1 and TP53)[29]. Cardiomyocytes can exhibit a non-canonical, profibrotic and prohypertrophic SASP and undergo senescence following mitochondrial dysfunction and persistent, length-independent telomeric DNA damage.[6] The panel therefore also incorporated pathway-informed genes representing mechanisms potentially relevant to this cardiomyocyte-specific phenotype. These included MT-ATP6, as an indicator of the mitochondrial oxidative-phosphorylation pathway implicated in cardiomyocyte senescence,[6] which undergoes distinct transcriptional upregulation and remodelling during stress-induced cardiomyocyte senescence[30]. IGF1R was included as a pathway-associated candidate because myocardial IGF1R expression increases with age, while experimental activation of IGF-1R signalling induces senescence-associated features in cardiomyocytes and cardiomyocyte-specific IGF1R deletion attenuates age-associated senescence phenotypes and adverse cardiac remodelling;[31] IRF3, a downstream mediator of cGAS–STING signalling that contributes to DNA-damage-induced senescence[32] and is a component of the recently derived 106-gene single-cell SenSet senescence signature panel[33]; NFKB1 was included as a pathway-informed component of NF-κB signalling, a central regulator of SASP production and the inflammatory feedback that reinforces persistent DNA damage and cellular senescence[34,35]; SIRT1 and TERF2, which are differentially expressed following senescence induction;[36,37] TERT, representing telomerase-dependent protection against telomere dysfunction and replicative senescence; and TP53BP1, a DNA-damage-response factor recruited to persistent dysfunctional-telomere foci during senescence.[38] PURPL, a p53-regulated long non-coding RNA associated with stress-induced senescence[39], was also included. These genes were included as mechanistically informed indicators of senescence-associated pathways rather than as uniformly upregulated or individually specific markers of senescent cardiomyocytes. **Fibrosis and inflammatory programme scoring:** To characterise the biological context of senescence-associated spatial regions, focused fibrosis and

inflammatory transcriptional programmes were quantified at the Visium spot level. These modules were designed to capture complementary aspects of post-myocardial-infarction tissue remodelling rather than to represent previously published fixed gene signatures. The fibrosis programme comprised 22 genes representing structural extracellular-matrix deposition, activated fibroblast and scar-associated states, matrix organisation and turnover, and pro-fibrotic/myofibroblast signalling: COL1A1, COL1A2, COL3A1, COL5A1, COL6A1, COL6A2, COL6A3, FN1, POSTN, DCN, LUM, THBS1, TNC, SPARC, CTHRC1, MMP2, MMP9, TIMP1, TGFB1, ACTA2, PDGFRA and PDGFRB. The panel therefore encompasses fibrillar and microfibrillar collagens involved in infarct scar formation; matricellular and extracellular-matrix proteins associated with activated cardiac fibroblasts and post-infarction remodelling; regulators of matrix turnover; and established components of fibroblast and myofibroblast activation.

The inflammatory programme comprised 23 genes representing chemokine and cytokine signalling, inflammatory activation, endothelial/leucocyte adhesion and myeloid/leucocyte-associated transcription: PTPRC, LST1, TYROBP, AIF1, FCER1G, CTSS, C1QA, C1QB, C1QC, CCL2, CCL3, CCL4, CXCL8, CXCL10, IL1B, IL6, TNF, NFKBIA, ICAM1, VCAM1, CD68, ITGAM and LYZ. This programme was used to provide transcriptional inflammatory context complementary to the independently derived cell-type abundance estimates; accordingly, it reflects both inflammatory signalling activity and the myeloid/leucocyte context of the tissue and was not interpreted as a direct measure of immune-cell abundance alone.

Gene selection was informed by established experimental and human literature describing extracellular-matrix remodelling, cardiac fibroblast activation, inflammatory signalling and immune-cell recruitment during myocardial infarction healing and adverse ventricular remodelling.[18,40-43] Programme scores were calculated at the individual spatial-spot level using Seurat AddModuleScore[44] with 24 expression bins. Genes unavailable in the expression assay for an individual sample were excluded from scoring for that sample, and gene matching was recorded as part of module-level quality control.

Custom gene panels were imported, and gene symbols were standardised before analysis by trimming whitespace, harmonising case, removing bracketed annotations

and standardising *BCL2* family nomenclature. Complete gene lists, provenance and gene-level supporting references are provided in **Supplementary Data**. Spot-level expression values were extracted for individual genes of interest, including *CDKN1A*, *CDKN2A*, selected fibrosis and immune-associated genes, and anti-apoptotic *BCL-2*-family genes. The anti-apoptotic *BCL-2*-family analysis included *BCL2*, *BCL2L1*, *BCL2L2*, *MCL1* and *BCL2A1*, with spots classified as positive if expression of at least one of these genes was detected. Spatial coordinates were recovered from Seurat tissue coordinates where available. Cell-type proportions inferred by cell2location[23] were extracted from the Kuppe et al. c2l_props assay[18] and merged with the spot-level expression, coordinate and metadata table using sample identity and cleaned spot barcodes. These cell-type estimates were generated as part of the original Kuppe et al. human myocardial infarction atlas and were not re-derived in the present study.

For pathology-zone analyses, each data point represented one spatial sample. Single-gene senescence markers and *BCL2*-family targets were treated as sparse features. For *CDKN1A*, *CDKN2A*, *BCL2*, *BCL2L1* and *BCL2L2*, detection frequency was calculated as the percentage of spots with detectable expression, defined as expression >0. Conditional expression intensity was calculated as the median expression among positive spots only. Spatial marker burden was calculated as the fraction of positive spots multiplied by the median expression among positive spots. The multi-gene senescence programme score was summarised across all spots because it represents a broader transcriptional programme rather than sparse detection of a single transcript.

Senescence-high spatial contexts were defined within each sample and pathology zone. For non-sparse programme scores, high spots were defined as the top quartile of expression within each sample-zone group. For sparse markers, including *CDKN2A* where the upper-quartile threshold could be zero, marker-positive spots were compared with marker-negative spots to avoid classifying zero-expression spots as high.

Spatial neighbourhood analyses were performed within pathology-zone sample groups. For each sample and senescence seed definition, Euclidean distances were calculated from spot coordinates. The neighbourhood radius was defined as twice the median nearest-neighbour distance within the corresponding sample-zone group.

Seed spots were defined using sparse-aware *CDKN1A* or *CDKN2A* positivity, or by top-quartile senescence programme score. Neighbouring spots were defined as non-seed spots located within the neighbourhood radius of at least one seed spot. All remaining non-seed spots were classified as other spots. Seed, neighbouring and other spot classes were mutually exclusive.

Statistical Analysis.

Mouse data are shown as individual animals with group means ± SEM. Comparisons between IR + Vehicle and IR + Navitoclax groups were performed using two-tailed unpaired t-tests with Welch's correction. Statistical testing for manuscript-facing spatial transcriptomic analyses was performed at sample level rather than spot level because Visium spots are spatially autocorrelated and do not represent independent biological replicates. This approach is consistent with spatial-analysis principles indicating that spatial transcriptomic observations violate classical assumptions of independence and are influenced by spatial scale, aggregation and spatial heterogeneity.[45] Pre-specified comparisons were performed on sample-level summaries using Wilcoxon tests for paired or two-group comparisons, or Kruskal-Wallis/Friedman tests where appropriate for multi-group comparisons. Multiple related comparisons were adjusted using Benjamini-Hochberg correction, and significance annotations in figures were based on adjusted *p*-values.

Data availability

The human myocardial spatial transcriptomic data analysed in this study were obtained from the publicly available dataset reported by Kuppe *et al*.[18] "Raw data generated by CellRanger and SpaceRanger pipelines are available through the Human Cell Atlas Data Portal at https://data.humancellatlas.org/explore/projects/e9f36305-d857-44a3-93f0-df4e6007dc97 and at the Zenodo data archive (https://zenodo.org/record/6578553, https://zenodo.org/record/6578617 and https://zenodo.org/record/6580069). Additional information is available from the corresponding author upon reasonable request.

Code availability

The specific code for the human myocardial spatial transcriptomic data analysed performed this study is available at **https://zenodo.org/records/21924094,**

Acknowledgements

This work was supported by the British Heart Foundation PG/25/12266. We thank Comparative Biology Centre at Newcastle University for assistance with animal work.

Competing interests

Eleftherios Zormpas is currently an employee of Translational Omics, Translational Sciences, GSK, Gunnels Wood Road, Stevenage, SG1 2NY, UK. All other authors declare no financial or non-financial competing interests.

Author contributions.

RER performed the animal experiments and animal data collection and analysis. EZ performed the spatial transcriptomic analyses. MCE contributed to the selection of the senescence panel. LM contributed to data quantification and validation. GDR, IS, SJC and STC contributed to manuscript preparation and study management. All authors contributed to study design and data interpretation and reviewed and approved the manuscript.

References

1 Alabas, O. A. *et al.* Statistics on mortality following acute myocardial infarction in 842 897 Europeans. *Cardiovasc Res* **116**, 149-157 (2020). https://doi.org:10.1093/cvr/cvz197

2 Garcia Rubira, J. C. *et al.* [Age is the independent prognostic factor in acute myocardial infarct. The clinical course of infarct in the elderly patient]. *An Med Interna* **12**, 61-64 (1995).

3 Shih, H., Lee, B., Lee, R. J. & Boyle, A. J. The aging heart and post-infarction left ventricular remodeling. *J Am Coll Cardiol* **57**, 9-17 (2011). https://doi.org:10.1016/j.jacc.2010.08.623

4 Hausenloy, D. J. & Yellon, D. M. Myocardial ischemia-reperfusion injury: a neglected therapeutic target. *J Clin Invest* **123**, 92-100 (2013). https://doi.org:10.1172/JCI62874

5 Walaszczyk, A. *et al.* Pharmacological clearance of senescent cells improves survival and recovery in aged mice following acute myocardial infarction. *Aging Cell* **18**, e12945 (2019). https://doi.org:10.1111/acel.12945

6 Anderson, R. *et al.* Length-independent telomere damage drives post-mitotic cardiomyocyte senescence. *EMBO J* **38**, EMBJ2018100492 (2019). https://doi.org:10.15252/embj.2018100492

7 von Zglinicki, T. Oxidative stress and cell senescence as drivers of ageing: Chicken and egg. *Ageing Res Rev* **102**, 102558 (2024). https://doi.org:10.1016/j.arr.2024.102558
8 Redgrave, R. E. *et al.* Senescent cardiomyocytes contribute to cardiac dysfunction following myocardial infarction. *NPJ Aging* **9**, 15 (2023). https://doi.org:10.1038/s41514-023-00113-5
9 Dookun, E. *et al.* Clearance of senescent cells during cardiac ischemia-reperfusion injury improves recovery. *Aging Cell* **19**, e13249 (2020). https://doi.org:10.1111/acel.13249
10 Salerno, N. *et al.* Pharmacological clearance of senescent cells improves cardiac remodeling and function after myocardial infarction in female aged mice. *Mech Ageing Dev* **208**, 111740 (2022). https://doi.org:10.1016/j.mad.2022.111740
11 Nakagawa, M. *et al.* Mechanisms by which late coronary reperfusion mitigates postinfarction cardiac remodeling. *Circ Res* **103**, 98-106 (2008). https://doi.org:10.1161/CIRCRESAHA.108.177568
12 Pluijmert, N. J., Bart, C. I., Bax, W. H., Quax, P. H. A. & Atsma, D. E. Effects on cardiac function, remodeling and inflammation following myocardial ischemia-reperfusion injury or unreperfused myocardial infarction in hypercholesterolemic APOE*3-Leiden mice. *Sci Rep* **10**, 16601 (2020). https://doi.org:10.1038/s41598-020-73608-w
13 Wilson, W. H. *et al.* Navitoclax, a targeted high-affinity inhibitor of BCL-2, in lymphoid malignancies: a phase 1 dose-escalation study of safety, pharmacokinetics, pharmacodynamics, and antitumour activity. *Lancet Oncol* **11**, 1149-1159 (2010). https://doi.org:10.1016/s1470-2045(10)70261-8
14 Montani, D. *et al.* Pulmonary arterial hypertension in patients treated by dasatinib. *Circulation* **125**, 2128-2137 (2012). https://doi.org:10.1161/circulationaha.111.079921
15 Hickson, L. J. *et al.* Senolytics decrease senescent cells in humans: Preliminary report from a clinical trial of Dasatinib plus Quercetin in individuals with diabetic kidney disease. *EBioMedicine* **47**, 446-456 (2019). https://doi.org:10.1016/j.ebiom.2019.08.069
16 Dutta, S. & Sengupta, P. Men and mice: Relating their ages. *Life Sci* **152**, 244-248 (2016). https://doi.org:10.1016/j.lfs.2015.10.025
17 Cui, S. *et al.* Postinfarction Hearts Are Protected by Premature Senescent Cardiomyocytes Via GATA 4-Dependent CCN 1 Secretion. *J Am Heart Assoc* **7**, e009111 (2018). https://doi.org:10.1161/JAHA.118.009111
18 Kuppe, C. *et al.* Spatial multi-omic map of human myocardial infarction. *Nature* **608**, 766-777 (2022). https://doi.org:10.1038/s41586-022-05060-x
19 Yang, T. *et al.* p16(INK4a) promotes myocardial ischemia-reperfusion injury by regulating bile acid transport via Slco1a4. *EMBO Rep* **27**, 1023-1056 (2026). https://doi.org:10.1038/s44319-025-00688-y
20 Gorgoulis, V. *et al.* Cellular Senescence: Defining a Path Forward. *Cell* **179**, 813-827 (2019). https://doi.org:10.1016/j.cell.2019.10.005
21 Sharpless, N. E. & DePinho, R. A. The INK4A/ARF locus and its two gene products. *Curr Opin Genet Dev* **9**, 22-30 (1999). https://doi.org:10.1016/s0959-437x(99)80004-5
22 Saul, D. *et al.* A new gene set identifies senescent cells and predicts senescence-associated pathways across tissues. *Nat Commun* **13**, 4827 (2022). https://doi.org:10.1038/s41467-022-32552-1

23 Kleshchevnikov, V. *et al.* Cell2location maps fine-grained cell types in spatial transcriptomics. *Nat Biotechnol* **40**, 661-671 (2022). https://doi.org:10.1038/s41587-021-01139-4
24 Zhu, Y. *et al.* The Achilles' heel of senescent cells: from transcriptome to senolytic drugs. *Aging Cell* **14**, 644-658 (2015). https://doi.org:10.1111/acel.12344
25 Zhu, Y. *et al.* Identification of a novel senolytic agent, navitoclax, targeting the Bcl-2 family of anti-apoptotic factors. *Aging Cell* **15**, 428-435 (2016). https://doi.org:10.1111/acel.12445
26 Saul, D. *et al.* Distinct senotypes in p16- and p21-positive cells across human and mouse aging tissues. *EMBO J* **44**, 7295-7325 (2025). https://doi.org:10.1038/s44318-025-00601-2
27 Chang, J. *et al.* Clearance of senescent cells by ABT263 rejuvenates aged hematopoietic stem cells in mice. *Nat Med* **22**, 78-83 (2016). https://doi.org:10.1038/nm.4010
28 Lonsdale, J. *et al.* The Genotype-Tissue Expression (GTEx) project. *Nature Genetics* **45**, 580-585 (2013). https://doi.org:10.1038/ng.2653
29 Fridman, A. L. & Tainsky, M. A. Critical pathways in cellular senescence and immortalization revealed by gene expression profiling. *Oncogene* **27**, 5975-5987 (2008). https://doi.org:10.1038/onc.2008.213
30 Camacho-Encina, M. *et al.* Cellular Senescence, Mitochondrial Dysfunction, and Their Link to Cardiovascular Disease. *Cells* **13** (2024). https://doi.org:10.3390/cells13040353
31 Ock, S. *et al.* Deletion of IGF-1 Receptors in Cardiomyocytes Attenuates Cardiac Aging in Male Mice. *Endocrinology* **157**, 336-345 (2016). https://doi.org:10.1210/en.2015-1709
32 Wu, Q. *et al.* IRF3 activates RB to authorize cGAS-STING-induced senescence and mitigate liver fibrosis. *Sci Adv* **10**, eadj2102 (2024). https://doi.org:10.1126/sciadv.adj2102
33 Hasanaj, E. *et al.* SenSet defines cell-type specific senescence signatures in the aged human lung. *The EMBO Journal* **45**, 3589-3638 (2026). https://doi.org:10.1038/s44318-026-00762-8
34 Chien, Y. *et al.* Control of the senescence-associated secretory phenotype by NF-κB promotes senescence and enhances chemosensitivity. *Genes Dev* **25**, 2125-2136 (2011). https://doi.org:10.1101/gad.17276711
35 Jurk, D. *et al.* Chronic inflammation induces telomere dysfunction and accelerates ageing in mice. *Nature Communications* **5**, 4172 (2014). https://doi.org:10.1038/ncomms5172
36 Spallarossa, P. *et al.* Doxorubicin induces senescence or apoptosis in rat neonatal cardiomyocytes by regulating the expression levels of the telomere binding factors 1 and 2. *Am J Physiol Heart Circ Physiol* **297**, H2169-2181 (2009). https://doi.org:10.1152/ajpheart.00068.2009
37 Tran, D. *et al.* Insulin-like growth factor-1 regulates the SIRT1-p53 pathway in cellular senescence. *Aging Cell* **13**, 669-678 (2014). https://doi.org:10.1111/acel.12219
38 Fagagna, F. d. A. d. *et al.* A DNA damage checkpoint response in telomere-initiated senescence. *Nature* **426**, 194-198 (2003). https://doi.org:10.1038/nature02118

39 Li, X. L. *et al.* Long Noncoding RNA PURPL Suppresses Basal p53 Levels and Promotes Tumorigenicity in Colorectal Cancer. *Cell Rep* **20**, 2408-2423 (2017). https://doi.org:10.1016/j.celrep.2017.08.041
40 Talman, V. & Ruskoaho, H. Cardiac fibrosis in myocardial infarction-from repair and remodeling to regeneration. *Cell Tissue Res* **365**, 563-581 (2016). https://doi.org:10.1007/s00441-016-2431-9
41 Frangogiannis, N. G. The inflammatory response in myocardial injury, repair, and remodelling. *Nat Rev Cardiol* **11**, 255-265 (2014). https://doi.org:10.1038/nrcardio.2014.28
42 Ruiz-Villalba, A. *et al.* Single-Cell RNA Sequencing Analysis Reveals a Crucial Role for CTHRC1 (Collagen Triple Helix Repeat Containing 1) Cardiac Fibroblasts After Myocardial Infarction. *Circulation* **142**, 1831-1847 (2020). https://doi.org:10.1161/circulationaha.119.044557
43 Kubota, A. & Frangogiannis, N. G. Macrophages in myocardial infarction. *Am J Physiol Cell Physiol* **323**, C1304-c1324 (2022). https://doi.org:10.1152/ajpcell.00230.2022
44 Hao, Y. *et al.* Integrated analysis of multimodal single-cell data. *Cell* **184**, 3573-3587.e3529 (2021). https://doi.org:https://doi.org/10.1016/j.cell.2021.04.048
45 Zormpas, E., Queen, R., Comber, A. & Cockell, S. J. Mapping the transcriptome: Realizing the full potential of spatial data analysis. *Cell* **186**, 5677-5689 (2023). https://doi.org:10.1016/j.cell.2023.11.003

Supplementary Files

This is a list of supplementary files associated with this preprint. Click to download.

- SupplementaryFigures.docx
- SupplementaryData1.xlsx